

Supporting information for:

## The Inherent Structural Instability: Concentration Dependent Transformation of Pyrogallarene to Pyrogallarene Lactones

Elina Kalenius,\* N. Kodiah Beyeh, J. Jänis, and Kari Rissanen\*

### Table of Contents

1. Experimental.....	2
2. Mass spectrometric data.....	4
2.1 Relative abundance of 1 as a function of stock solution aging time ....	4
2.2 Profile spectra measured from 10uM solutions.....	5
2.3 Relative intensity of 1 and fragments as a function of stock solution aging time .....	6
2.4 Composition, theoretical and experimental mass values and mass accuracies of ions.....	7
2.5 CID dissociation of 2 and 3. ....	8
2.6 CID fragmentation pathways for ions 2 and 3. ....	9
2.7 Composition, theoretical and experimental mass values and mass accuracies of the CID fragments from 2.. ....	10
2.8 Composition, theoretical and experimental mass values and mass accuracies of the CID fragments from 3.. ....	11
3. NMR Experiments: <sup>1</sup> H NMR in DMSO, <sup>1</sup> H <sup>1</sup> H COSY and <sup>1</sup> H <sup>1</sup> H NOESY NMR in CD <sub>3</sub> OD.....	12
4. IR Spectra .....	16
5. DFT Optimizations .....	17
6. References.....	20

## 1. Experimental

The synthesis and characterization of pyrogallarene **1** have been reported earlier.<sup>1</sup> The pyrogallarene **1** was dissolved in methanol or acetonitrile. The final samples were prepared in MeOH.

The exact mass measurements, profile spectra measurements and H/D exchange reactions were performed by using an APEX Qe Fourier transform ion cyclotron resonance (FT-ICR) mass spectrometer equipped with 4.7 T superconducting magnet, Infinity® ICR cell, AP2 electrospray ion source and pre-cell quadrupole interface. The measurements and data handling were accomplished with Bruker XMASS software, version 6.0.2. The mass spectra were externally calibrated with an ES tuning mix (Hewlett Packard, Palo Alto, CA). The composition of the ions was confirmed by comparing the experimental monoisotopic  $m/z$  values and isotopic patterns with the theoretical values calculated on the basis of natural abundances. For accurate mass experiments for CID fragments the precursor ions were isolated, activated (cc-trap 15 to 35 V) and allowed to collide with Ar background gas in the pre-quadrupole. After that the ions were detected in the ICR cell. The compositions of the fragment ions were confirmed by accurate mass measurements with mass accuracy from -0.4 ppm to -6.4 ppm.

In H/D exchange ion-molecule reactions deuterated methanol (MeOD) was selected as a reagent and introduced to the ICR cell from a separate volume through an adjustable needle valve. MeOD gas flow, from volume to cell, was set to keep the cell pressure at elevated state of  $5 \cdot 10^{-8}$  Torr. The precursor ions were isolated in the ICR cell by using correlated harmonic excitation fields<sup>2</sup> and single frequency excitation shots were used to obtain monoisotopic isolation of the precursor ion. Isolated ions were allowed to react with MeOD by ranging the pumping delay times from 30 to 300 s. Sixteen scans were collected when reaction delays were 60 s or less, six scans when reaction delays were longer than 60 s and two scans when reaction delay was 300 s. The variation in the number of scans did not influence the information gathered from the resulting spectra.

The MS<sup>n</sup> CID for dissociation route determination was performed by using Bruker Esquire 3000 plus QIT mass spectrometer (Bruker Daltonik, Bremen Germany) equipped with an ESI source. The sample was introduced to the ion source at a flow rate of  $150 \mu\text{L h}^{-1}$ . N<sub>2</sub> (LC-MS-NGM 11 nitrogen generator, Bruker Daltonik) was used as a nebulizing (3 psi) and counter-current ( $2 \text{ L min}^{-1}$ ) drying gas. He (grade 5.6, AGA Espoo, Finland) was used as the buffer/collision gas. The fragmentation amplitudes from 0.30 to 0.70 were used. The Instrument was controlled and the data were processed by using a Bruker Daltonics Compass 1.1 for Esquire/HCT. Each spectrum was an average of spectra collected within 1 min, each of these containing 24 individual scans that were averaged before being sent from the instrument to data system.

The <sup>1</sup>H NMR spectra were recorded by using Bruker Avance DRX 500 FT NMR spectrometer operating at 500 MHz. Measurements were done in CD<sub>3</sub>OD and DMSO-*d*<sub>6</sub> at 30 °C. For the experiment, a 5 μM MeOH solution of compound **1** was prepared (10 mg in 3L) and left to stand for 2h. The MeOH was then evaporated and the residue was dried. The sample was dissolved in 0.6 mL CD<sub>3</sub>OD and the <sup>1</sup>H NMR was measured. The sampled NMR tube was left to stand at room temperature and the <sup>1</sup>H NMR was again measured after 7 days and 25 days respectively.

For the measurement of IR spectra 20  $\mu\text{M}$  and 2.5mM solutions of **1** were prepared in MeOH. After aging time, the solvent was evaporated and the spectra were recorded in KBr tablets by using Bruker Vertex 70 FT-IR spectrometer. The spectra were processed by using OPUS 6.5 software.

The optimizations of **1** and the decomposition products were carried out using Gaussian 09,<sup>3</sup> and hybrid density functional B3LYP/6-311G(d,p). The energy minimum was confirmed by the frequency calculations (only real frequencies were obtained).

## 2. Mass Spectrometric Data

### 2.1 Relative abundance of **1** as a function of stock solution aging time

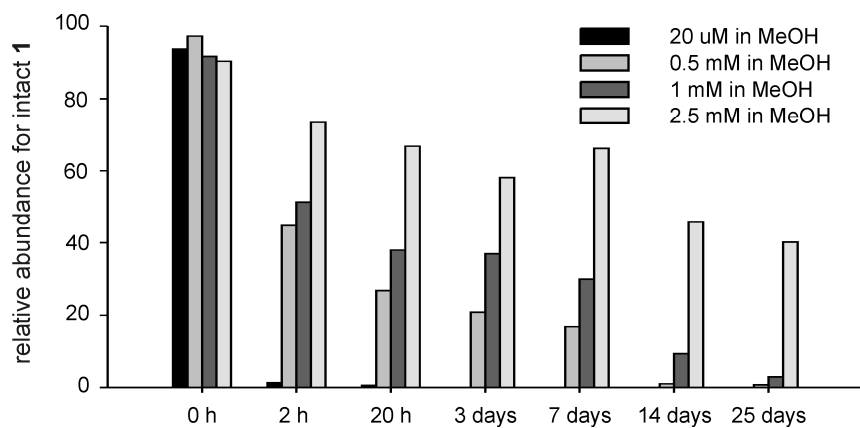


Figure S11. Relative abundance of **1** in the mass spectra as measured from 10  $\mu$ M MeOH solutions prepared from the aged stock solutions of 20  $\mu$ M, 0.5 mM, 1mM and 2.5 mM MeOH.

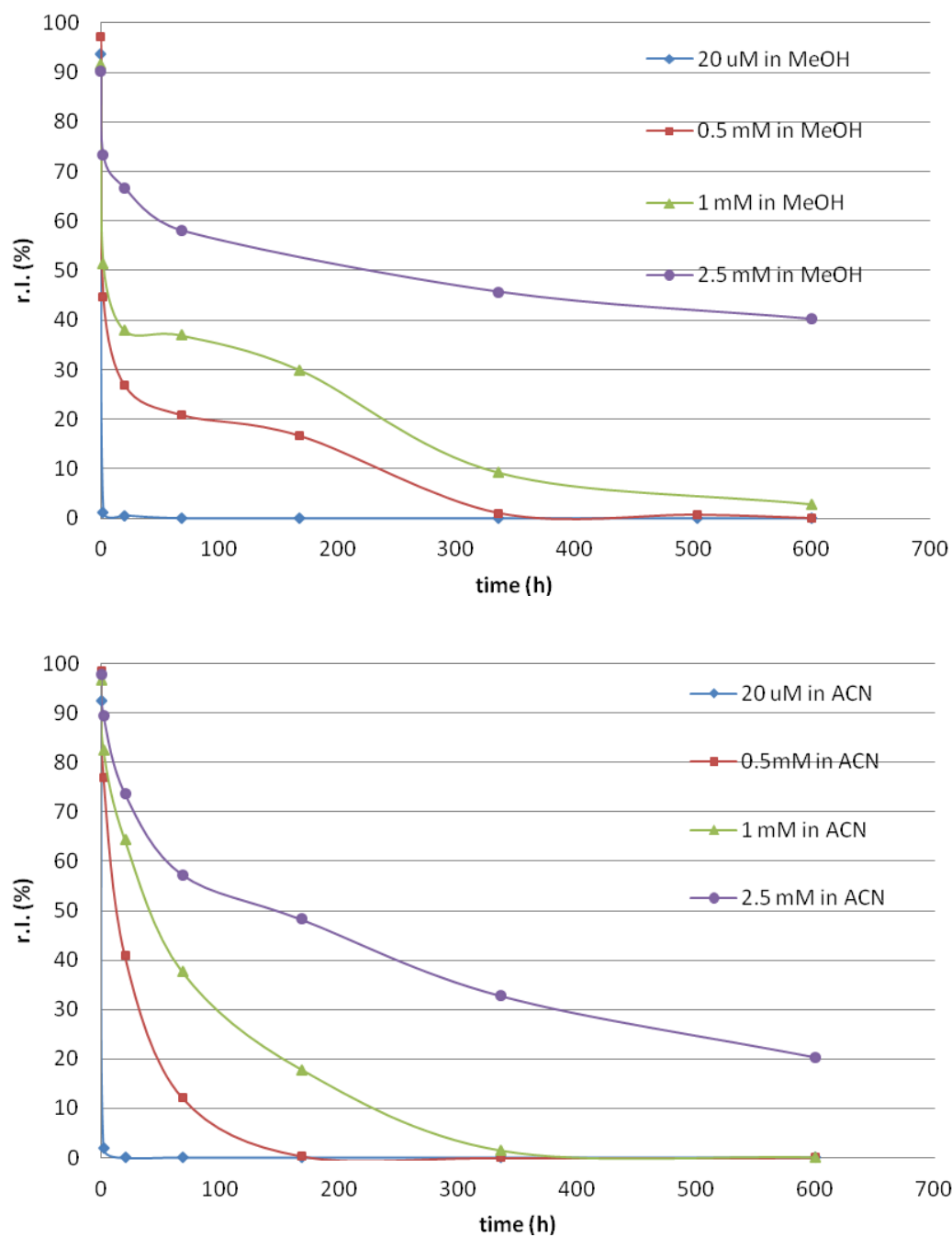


Figure SI2. Relative abundance of **1** as a function of stock solution aging time. Stock solutions in MeOH (up) and ACN (down).

## 2.2 Profile spectra measured from 10 $\mu$ M solutions

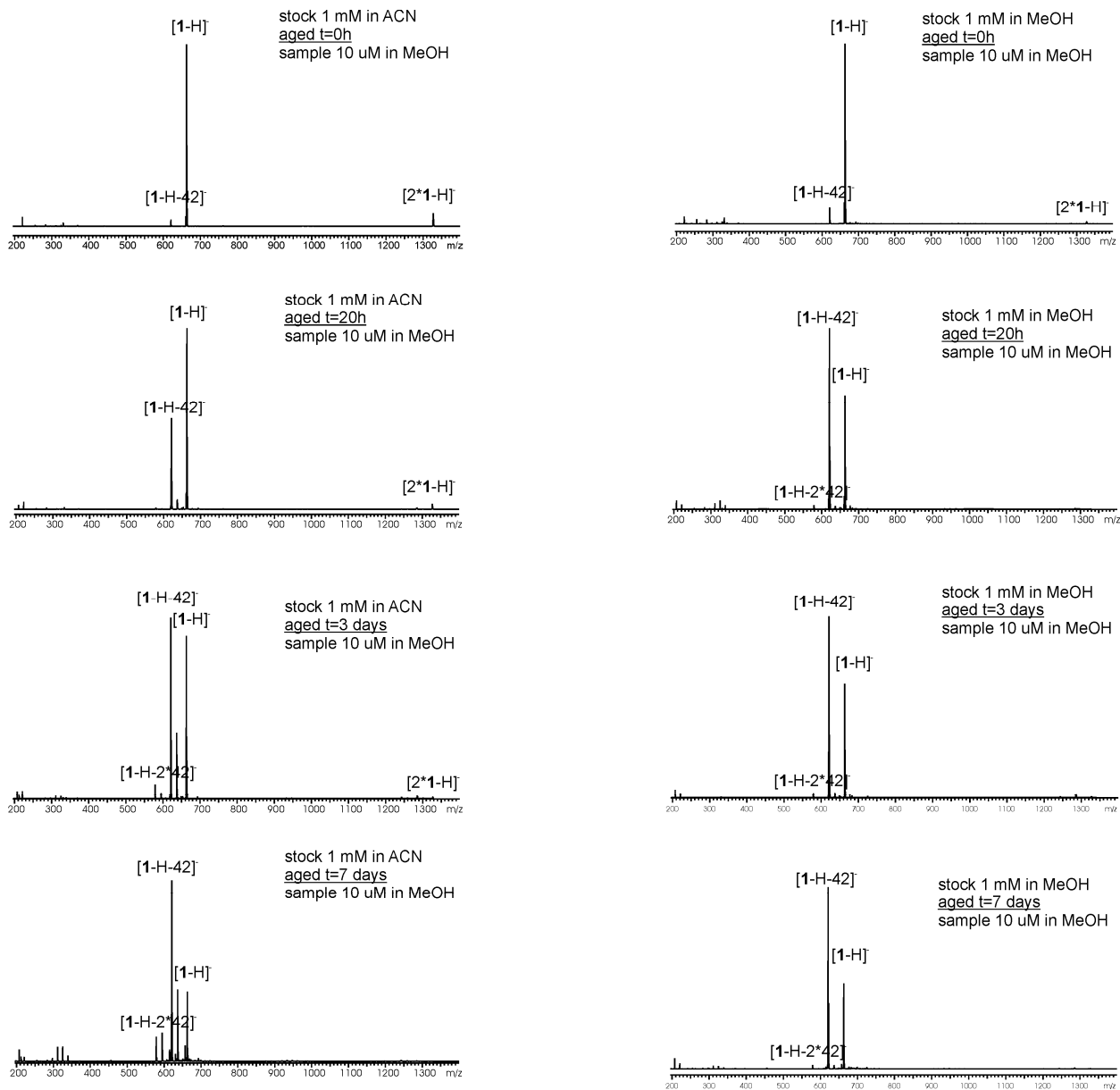


Figure SI3. Profile spectra measured from 10  $\mu$ M MeOH solutions, which were prepared from 1 mM ACN (left) or MeOH (right) stock solutions.

### 2.3 Relative intensity of **1** and fragments as a function of stock solution aging time

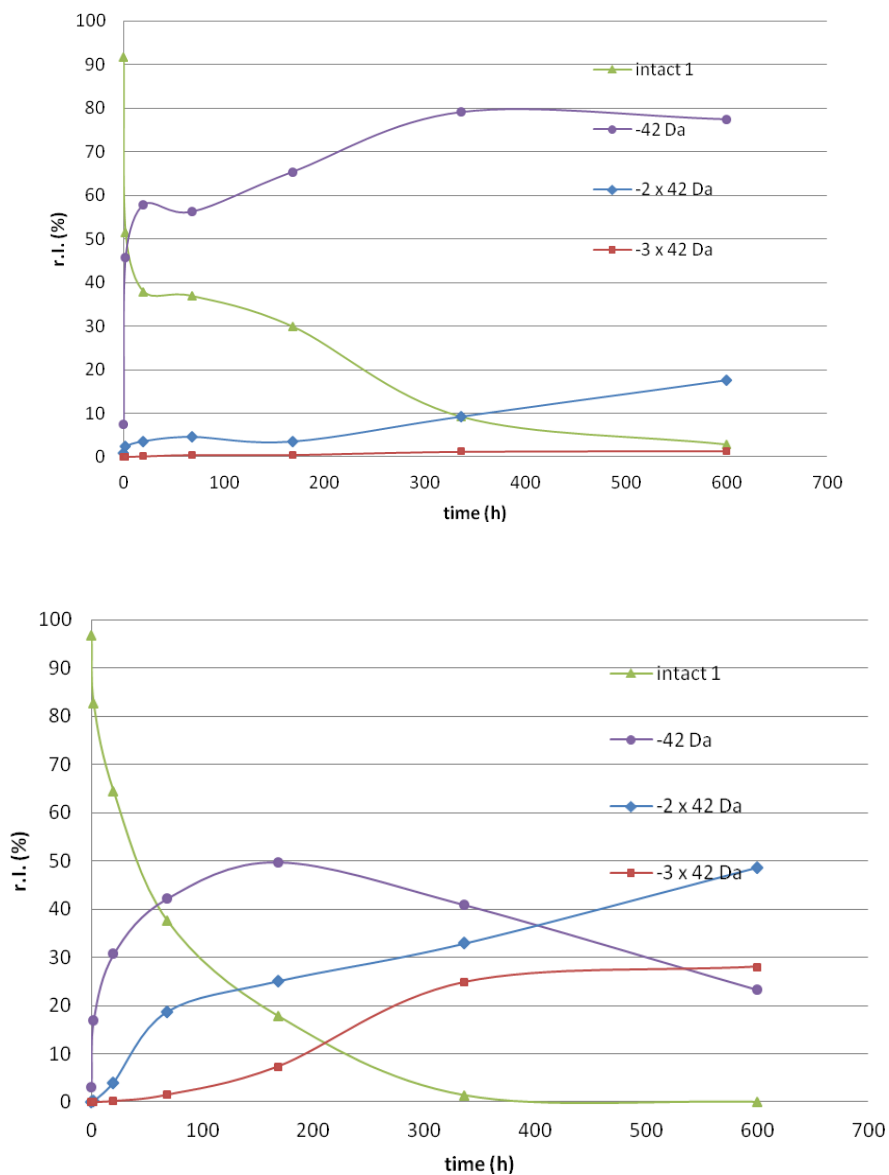


Figure SI4. Relative intensity of **1** and its fragments as a function of stock solution aging time. Stock solutions (1 mM) in MeOH (up) and ACN (down).

## 2.4 Composition, theoretical and experimental mass values and mass accuracies of ions

Table SII. Compositions, theoretical and experimental mass values and mass accuracies of ions. For comparison values which would result from propene (C<sub>3</sub>H<sub>6</sub>) elimination are also presented (grey).

<b>Ion</b>	<b>composition</b>	<b>theor (m/z)</b>	<b>exp (m/z)</b>	<b>Δ (m/z)</b>	<b>Δ (ppm)</b>
[1-H] <sup>-</sup>	C <sub>36</sub> H <sub>39</sub> O <sub>12</sub>	663.24468	663.239372	0.0053	8.0031
[1-H-C <sub>2</sub> H <sub>2</sub> O] <sup>-</sup>	C <sub>34</sub> H <sub>37</sub> O <sub>11</sub>	621.234115	621.233866	0.0002	0.4008
[1-H-2*C <sub>2</sub> H <sub>2</sub> O] <sup>-</sup>	C <sub>32</sub> H <sub>35</sub> O <sub>10</sub>	579.22355	579.22196	0.0016	2.7451
[1-H-C <sub>3</sub> H <sub>6</sub> ] <sup>-</sup>	C <sub>33</sub> H <sub>33</sub> O <sub>12</sub>	621.19773		-0.0361	-58.1715
[1-H-2*C <sub>3</sub> H <sub>6</sub> ] <sup>-</sup>	C <sub>30</sub> H <sub>27</sub> O <sub>12</sub>	579.15078		-0.0712	-122.9041
[1-H-C <sub>2</sub> H <sub>2</sub> O-C <sub>3</sub> H <sub>6</sub> ] <sup>-</sup>	C <sub>31</sub> H <sub>31</sub> O <sub>11</sub>	579.187165		-0.0348	-60.0756
[1+Na] <sup>+</sup>	C <sub>36</sub> H <sub>40</sub> O <sub>12</sub> Na <sub>1</sub>	687.241225	687.24122	0.0000	0.0073
[1+Na-C <sub>3</sub> H <sub>6</sub> ] <sup>+</sup>	C <sub>33</sub> H <sub>34</sub> O <sub>12</sub> Na <sub>1</sub>	645.19428		-0.0331	-51.3256
[1+Na-C <sub>2</sub> H <sub>2</sub> O] <sup>+</sup>	C <sub>34</sub> H <sub>38</sub> O <sub>11</sub> Na <sub>1</sub>	645.23066	645.22739	0.0033	5.0680
[1+Na-2*C <sub>3</sub> H <sub>6</sub> ] <sup>+</sup>	C <sub>30</sub> H <sub>28</sub> O <sub>12</sub> Na <sub>1</sub>	603.14733		-0.0730	-121.0401
[1+Na-C <sub>3</sub> H <sub>6</sub> -C <sub>2</sub> H <sub>2</sub> O] <sup>+</sup>	C <sub>31</sub> H <sub>32</sub> O <sub>11</sub> Na <sub>1</sub>	603.18371		-0.0366	-60.7112
[1+Na-2*C <sub>2</sub> H <sub>2</sub> O] <sup>+</sup>	C <sub>32</sub> H <sub>36</sub> O <sub>10</sub> Na <sub>1</sub>	603.22010	603.22033	-0.0002	-0.3896

### 2.5 CID dissociation of 2 and 3.

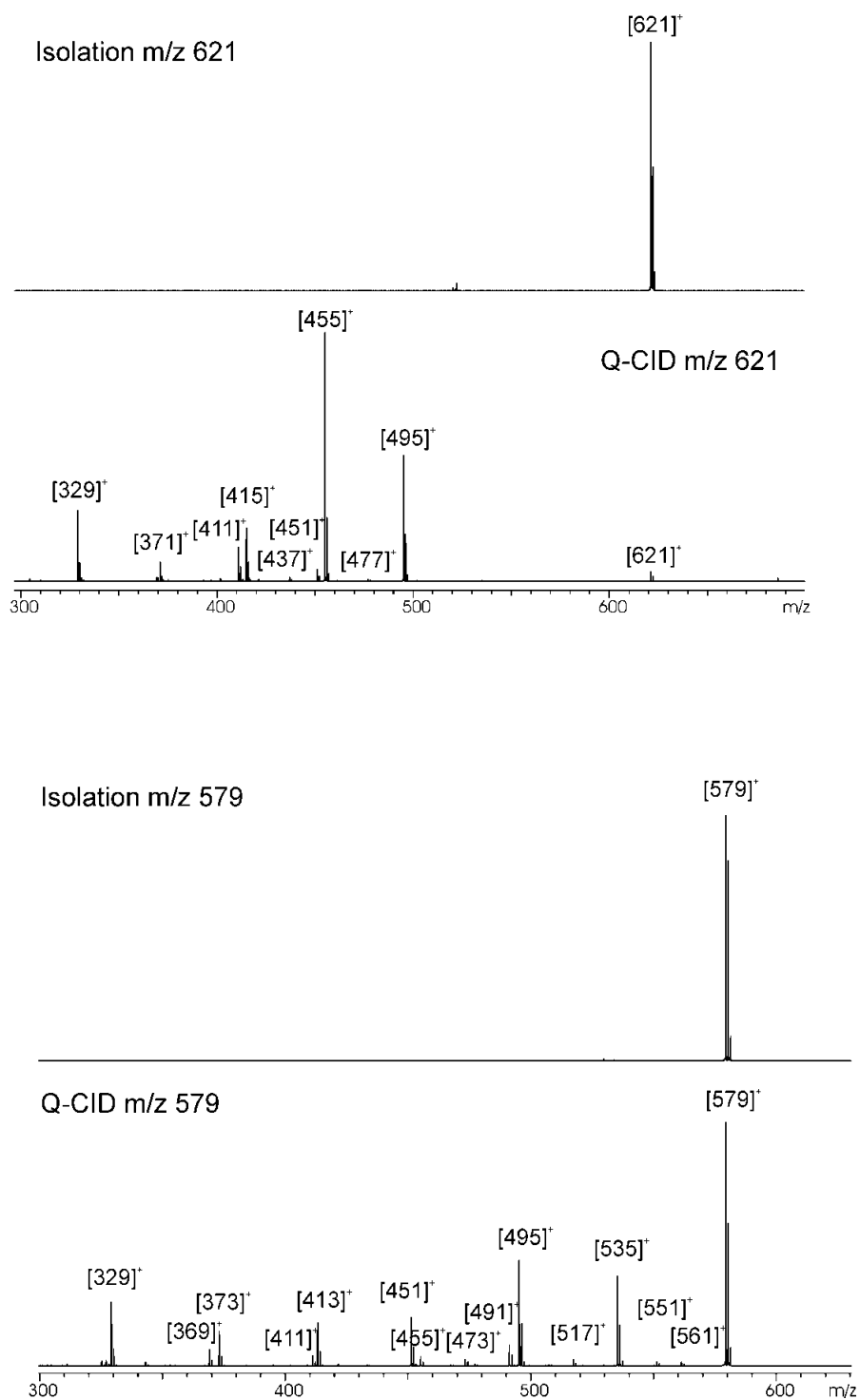


Figure SI5. CID dissociation of a)  $[1-H-42]^-$  and b)  $[1-H-2*42]^-$ .

### 2.6 CID fragmentation pathways for ions 2 and 3.

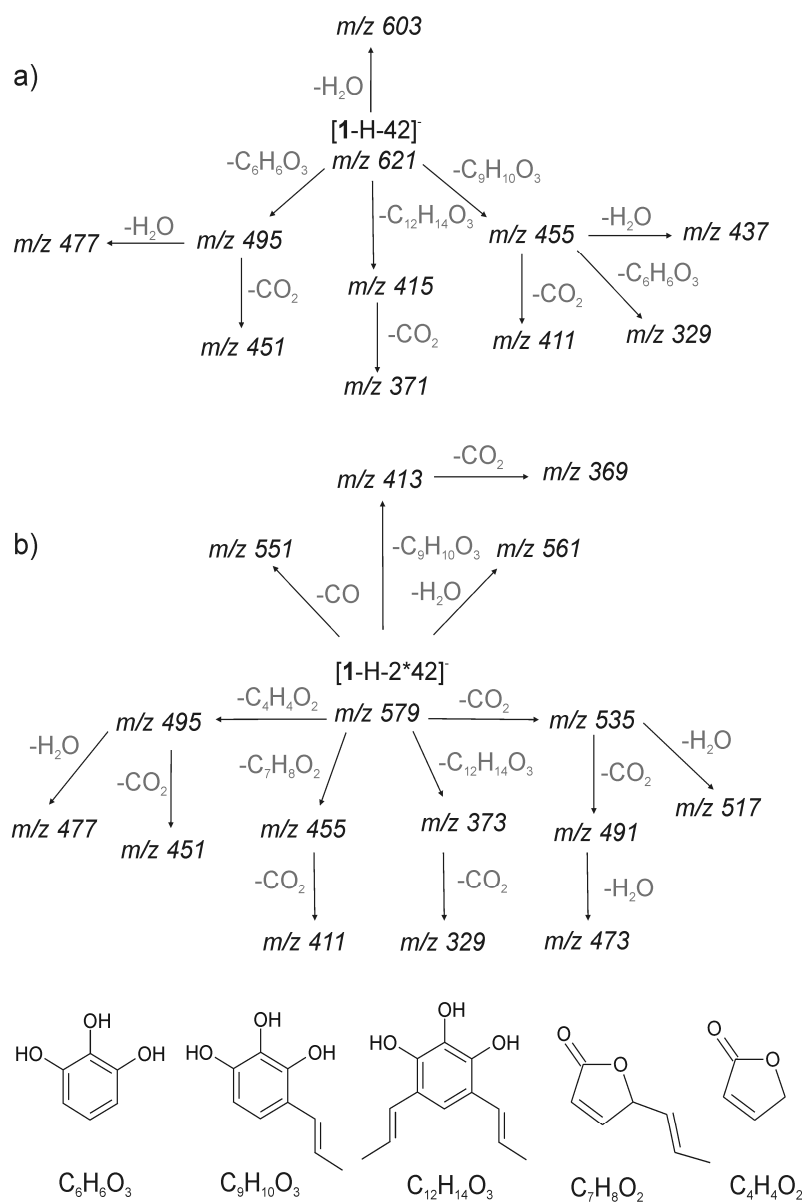


Figure SI6. CID fragmentation pathways for ions a) [1-H-42]<sup>-</sup> and b) [1-H-2\*42]<sup>-</sup>.

## 2.7 Composition, theoretical and experimental mass values and mass accuracies of the CID fragments from 2.

Table SI2. Compositions, theoretical and experimental mass values and mass accuracies of the CID fragments from  $m/z$  621 ([1-H-42]<sup>-</sup>).

Ion	composition	theor (m/z)	exp (m/z)	$\Delta$ (Da)	$\Delta$ (ppm)
[1-C <sub>2</sub> H <sub>2</sub> O-H]-	C <sub>34</sub> H <sub>37</sub> O <sub>11</sub>	621.234136	621.234506	-0.0004	-0.60
[1-C <sub>2</sub> H <sub>2</sub> O-H-H <sub>2</sub> O]-	C <sub>34</sub> H <sub>35</sub> O <sub>10</sub>	603.223571	603.223103	0.0005	0.78
[1-C <sub>2</sub> H <sub>2</sub> O-H-C <sub>6</sub> H <sub>6</sub> O <sub>3</sub> ]-	C <sub>28</sub> H <sub>31</sub> O <sub>8</sub>	495.202442	495.202933	-0.0005	-0.99
[1-C <sub>2</sub> H <sub>2</sub> O-H-C <sub>6</sub> H <sub>6</sub> O <sub>3</sub> -H <sub>2</sub> O]-	C <sub>28</sub> H <sub>29</sub> O <sub>7</sub>	477.191877	477.193196	-0.0013	-2.76
[1-C <sub>2</sub> H <sub>2</sub> O-H-C <sub>9</sub> H <sub>10</sub> O <sub>3</sub> ]-	C <sub>25</sub> H <sub>27</sub> O <sub>8</sub>	455.171141	455.17252	-0.0014	-3.03
[1-C <sub>2</sub> H <sub>2</sub> O-H-C <sub>6</sub> H <sub>6</sub> O <sub>3</sub> -CO <sub>2</sub> ]-	C <sub>27</sub> H <sub>31</sub> O <sub>6</sub>	451.212612	451.21367	-0.0011	-2.34
[1-C <sub>2</sub> H <sub>2</sub> O-H-C <sub>9</sub> H <sub>10</sub> O <sub>3</sub> -H <sub>2</sub> O]-	C <sub>25</sub> H <sub>25</sub> O <sub>7</sub>	437.160577	437.160713	-0.0001	-0.31
[1-C <sub>2</sub> H <sub>2</sub> O-H-C <sub>12</sub> H <sub>14</sub> O <sub>3</sub> ]-	C <sub>22</sub> H <sub>23</sub> O <sub>8</sub>	415.139841	415.139931	-0.0001	-0.22
[1-C <sub>2</sub> H <sub>2</sub> O-H-C <sub>9</sub> H <sub>10</sub> O <sub>3</sub> -CO <sub>2</sub> ]-	C <sub>24</sub> H <sub>27</sub> O <sub>6</sub>	411.181312	411.181333	0.0000	-0.05
[1-C <sub>2</sub> H <sub>2</sub> O-H-C <sub>12</sub> H <sub>14</sub> O <sub>3</sub> -CO <sub>2</sub> ]-	C <sub>21</sub> H <sub>23</sub> O <sub>6</sub>	371.150012	371.150919	-0.0009	-2.44
[1-C <sub>2</sub> H <sub>2</sub> O-H-C <sub>9</sub> H <sub>10</sub> O <sub>3</sub> -C <sub>6</sub> H <sub>6</sub> O <sub>3</sub> ]-	C <sub>19</sub> H <sub>21</sub> O <sub>5</sub>	329.139447	329.140096	-0.0006	-1.97

## 2.8 Composition, theoretical and experimental mass values and mass accuracies of the CID fragments from 3.

Table SI3. Compositions, theoretical and experimental mass values and mass accuracies of the CID fragments from  $m/z$  579 ([1-H-2x42]<sup>-</sup>).

Ion	composition	theor (m/z)	exp (m/z)	$\Delta$ (Da)	$\Delta$ (ppm)
[1-2*C <sub>2</sub> H <sub>2</sub> O-H]-	C <sub>32</sub> H <sub>35</sub> O <sub>10</sub>	579.223571	579.221219	0.0024	4.06
[1-2*C <sub>2</sub> H <sub>2</sub> O-H-H <sub>2</sub> O]-	C <sub>32</sub> H <sub>33</sub> O <sub>9</sub>	561.213006	561.213318	-0.0003	-0.56
[1-2*C <sub>2</sub> H <sub>2</sub> O-H-C <sub>4</sub> H <sub>4</sub> O <sub>2</sub> ]-	C <sub>28</sub> H <sub>31</sub> O <sub>8</sub>	495.202442	495.203547	-0.0011	-2.23
[1-2*C <sub>2</sub> H <sub>2</sub> O-H-CO <sub>2</sub> ]-	C <sub>31</sub> H <sub>35</sub> O <sub>8</sub>	535.233742	535.235847	-0.0021	-3.93
[1-2*C <sub>2</sub> H <sub>2</sub> O-H-C <sub>9</sub> H <sub>10</sub> O <sub>3</sub> ]-	C <sub>23</sub> H <sub>25</sub> O <sub>7</sub>	413.160577	413.163231	-0.0027	-6.42
[1-2*C <sub>2</sub> H <sub>2</sub> O-H-CO]-	C <sub>31</sub> H <sub>35</sub> O <sub>9</sub>	551.228656	551.231881	-0.0032	-5.85
[1-2*C <sub>2</sub> H <sub>2</sub> O-H-C <sub>4</sub> H <sub>4</sub> O <sub>2</sub> -H <sub>2</sub> O]-	C <sub>28</sub> H <sub>29</sub> O <sub>7</sub>	477.191877	477.192366	-0.0005	-1.02
[1-2*C <sub>2</sub> H <sub>2</sub> O-H-C <sub>4</sub> H <sub>4</sub> O <sub>2</sub> -CO <sub>2</sub> ]-	C <sub>27</sub> H <sub>31</sub> O <sub>6</sub>	451.212612	451.214836	-0.0022	-4.93
[1-2*C <sub>2</sub> H <sub>2</sub> O-H-C <sub>9</sub> H <sub>10</sub> O <sub>3</sub> -CO <sub>2</sub> ]-	C <sub>22</sub> H <sub>25</sub> O <sub>5</sub>	369.170747	369.170894	-0.0001	-0.40
[1-2*C <sub>2</sub> H <sub>2</sub> O-H-CO <sub>2</sub> -H <sub>2</sub> O]-	C <sub>31</sub> H <sub>33</sub> O <sub>7</sub>	517.223177	517.224373	-0.0012	-2.31
[1-2*C <sub>2</sub> H <sub>2</sub> O-H-2*CO <sub>2</sub> ]-	C <sub>30</sub> H <sub>35</sub> O <sub>6</sub>	491.243912	491.245731	-0.0018	-3.70
[1-2*C <sub>2</sub> H <sub>2</sub> O-H-2*CO <sub>2</sub> -H <sub>2</sub> O]-	C <sub>30</sub> H <sub>33</sub> O <sub>5</sub>	473.233348	473.233350	0.0000	-0.004
[1-2*C <sub>2</sub> H <sub>2</sub> O-H-C <sub>7</sub> H <sub>8</sub> O <sub>2</sub> ]-	C <sub>25</sub> H <sub>27</sub> O <sub>8</sub>	455.171141	455.173113	-0.0020	-4.33
[1-2*C <sub>2</sub> H <sub>2</sub> O-H-C <sub>12</sub> H <sub>14</sub> O <sub>3</sub> ]-	C <sub>20</sub> H <sub>21</sub> O <sub>7</sub>	373.129277	373.130227	-0.0009	-2.55
[1-2*C <sub>2</sub> H <sub>2</sub> O-H-C <sub>12</sub> H <sub>14</sub> O <sub>3</sub> -CO <sub>2</sub> ]-	C <sub>19</sub> H <sub>25</sub> O <sub>5</sub>	329.138800	329.140501	-0.0017	-5.17
[1-2*C <sub>2</sub> H <sub>2</sub> O-H-C <sub>7</sub> H <sub>8</sub> O <sub>2</sub> -CO <sub>2</sub> ]-	C <sub>24</sub> H <sub>27</sub> O <sub>6</sub>	411.181312	411.181913	-0.0006	-1.46

### 3. NMR Experiments: $^1\text{H}$ NMR in DMSO, $^1\text{H}$ $^1\text{H}$ COSY and $^1\text{H}$ $^1\text{H}$ NOESY NMR in $\text{CD}_3\text{OD}$

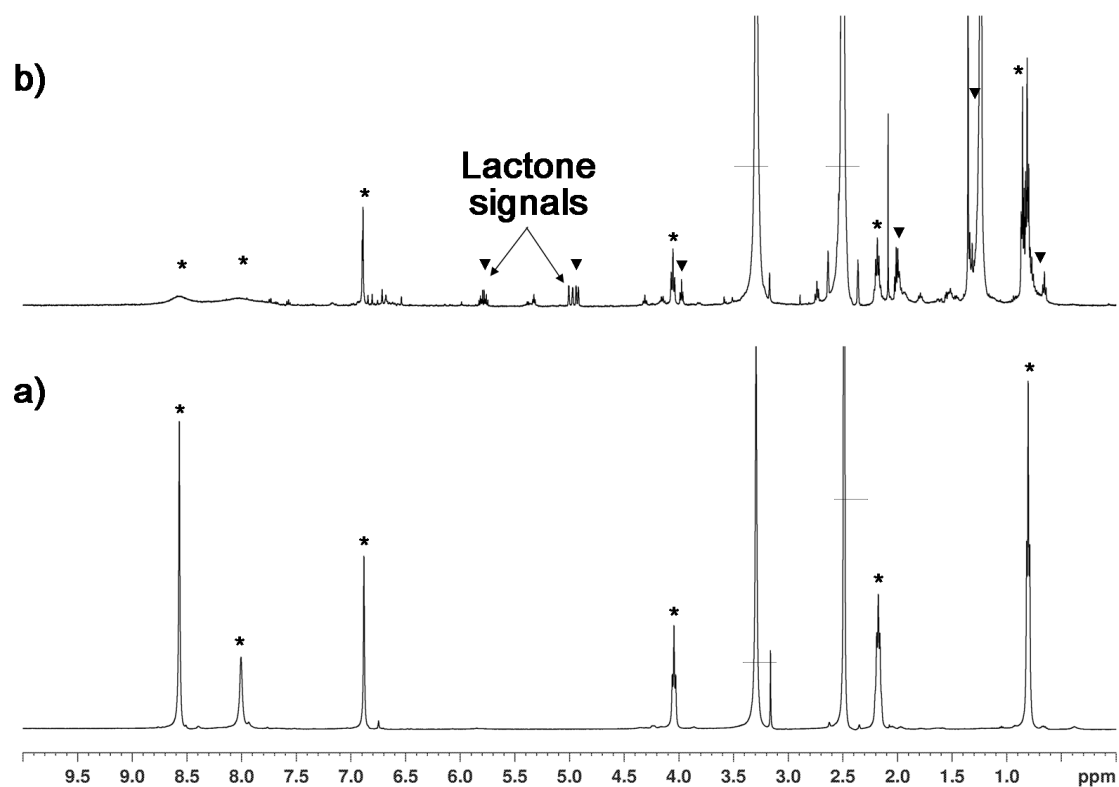


Figure SI7.  $^1\text{H}$  NMR of **1** in  $\text{DMSO-}d_6$  a) immediately, b) after standing  $5\ \mu\text{M}$  solution in  $\text{MeOH}$  for 2h. (\*) correspond to **1** in normal form and (▼) correspond to the new species.

$^1\text{H}$   $^1\text{H}$  COSY NMR in  $\text{CD}_3\text{OD}$

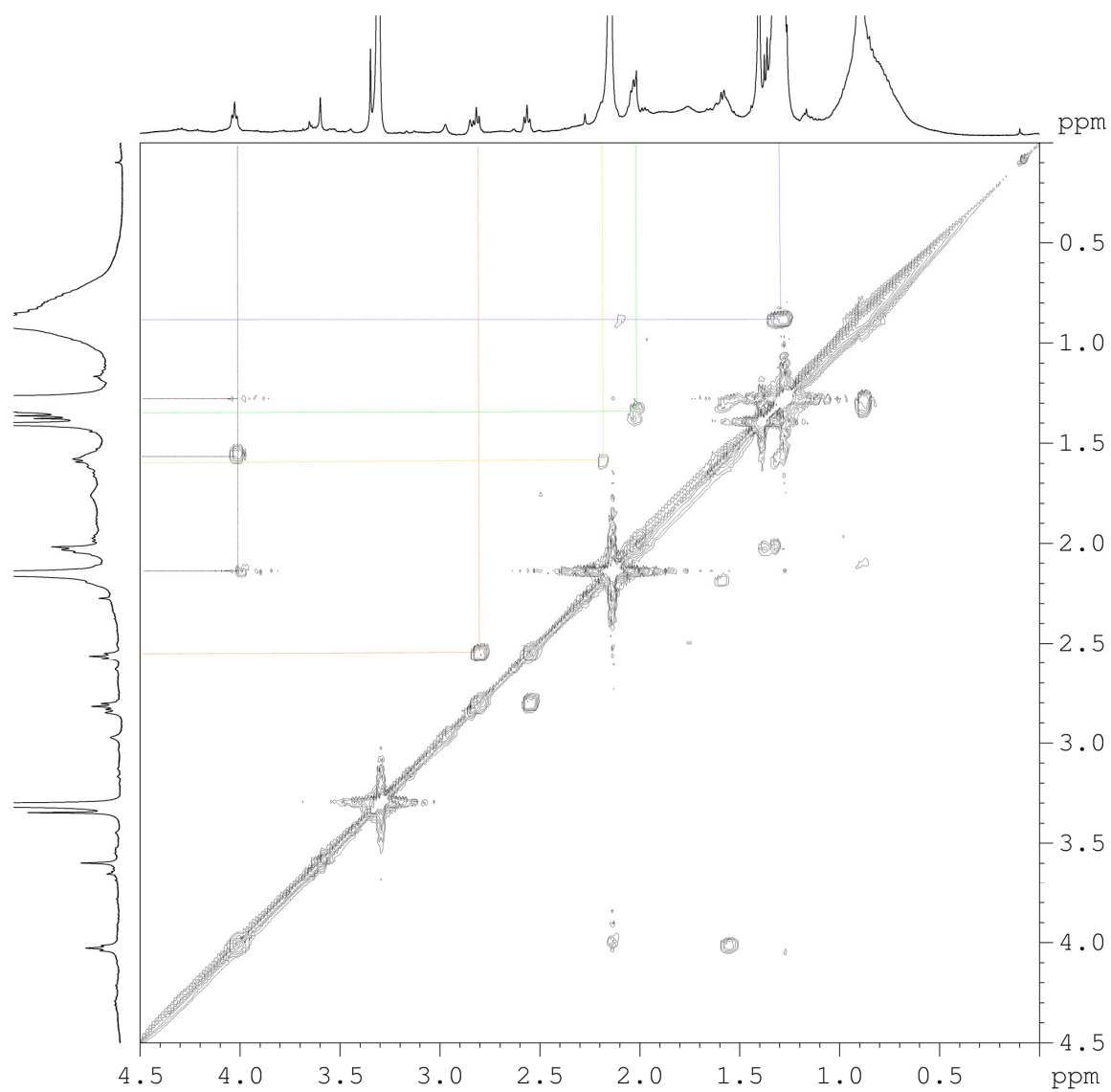


Figure SI8.  $^1\text{H}$   $^1\text{H}$  COSY NMR in  $\text{CD}_3\text{OD}$  of pyrogallarene **1** after 25 days.

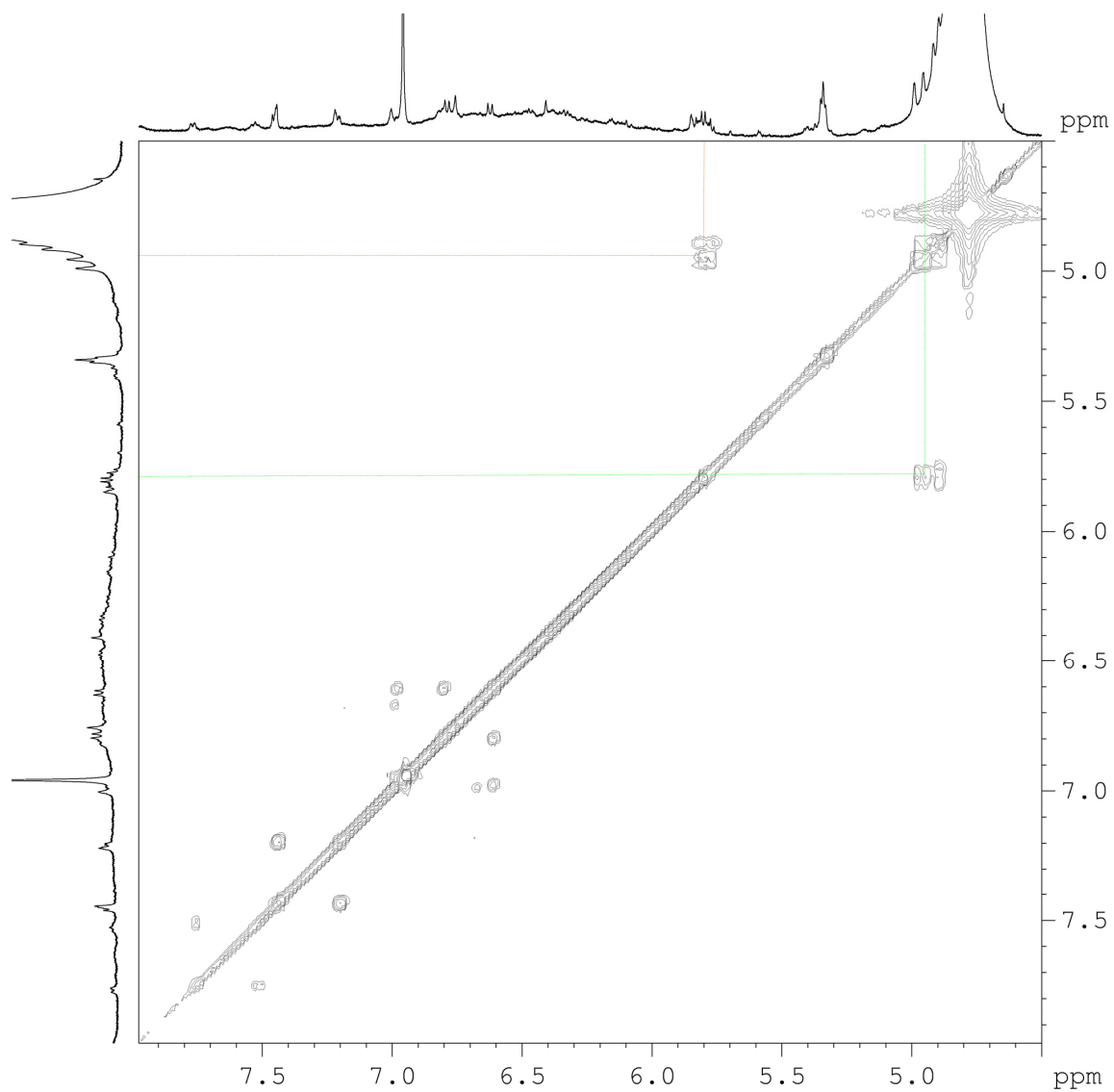


Figure SI9.  $^1\text{H}$   $^1\text{H}$  COSY NMR in  $\text{CD}_3\text{OD}$  of pyrogallarene **1** after 25 days.  
 $^1\text{H}$   $^1\text{H}$  NOESY NMR in  $\text{CD}_3\text{OD}$

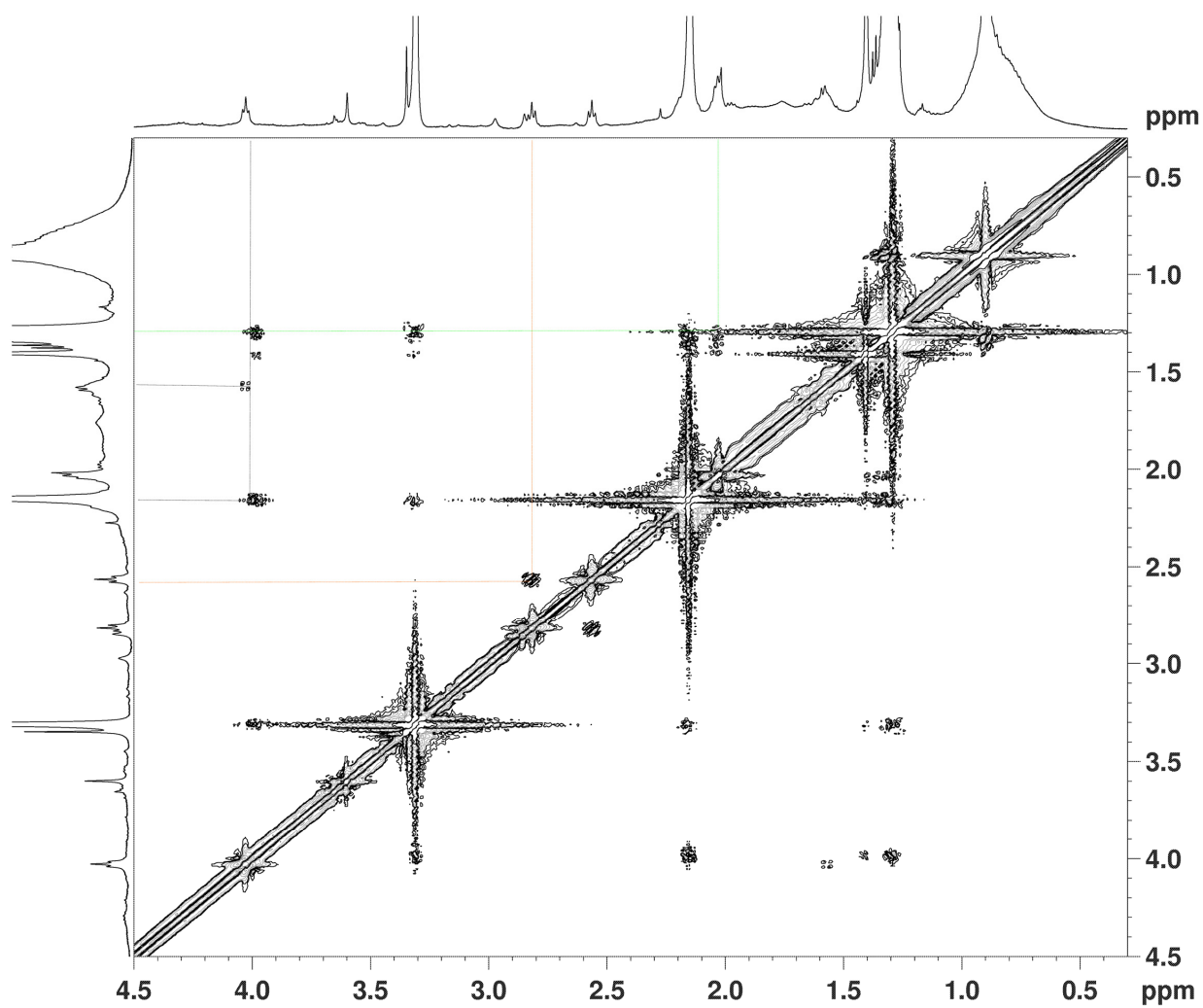


Figure SI10.  $^1\text{H}$   $^1\text{H}$  NOESY NMR in  $\text{CD}_3\text{OD}$  of pyrogallarene **1** after 25 days.

#### 4. IR experiments

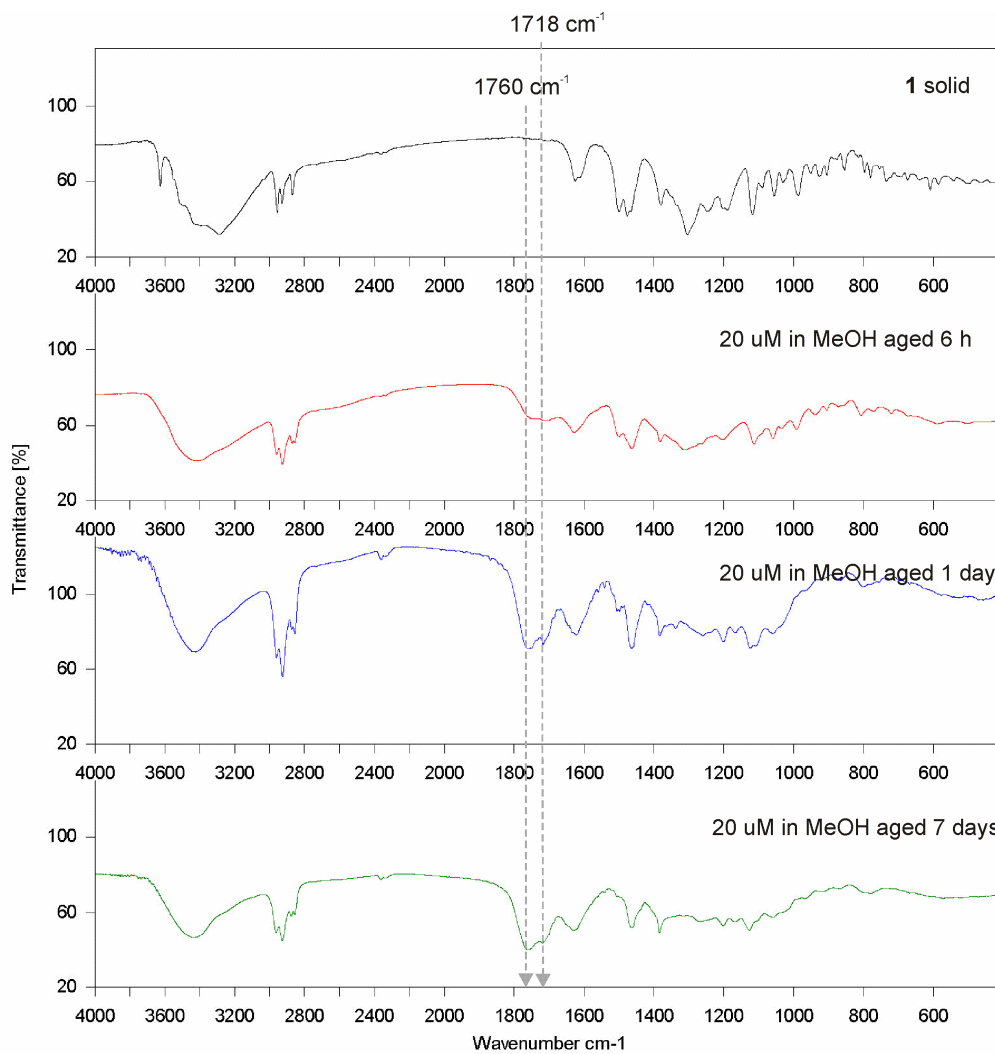


Figure SI11. IR spectra measured from solid **1** and  $20 \mu\text{M}$  MeOH solution of **1** after 6h, 1 day and 7 days aging followed by solvent evaporation.

## 5. DFT Optimizations

The DFT optimizations on monolactone **2** results in three distinct conformations: one with 4 intramolecular H-bonds (structure 2a in supporting material) and two with 3 H-bonds (structures 2b and 2c). Despite the larger number of H-bonds in 2a, it is not the lowest energy conformation. The formation of 4 H-bonds cause rupture of the cyclic orientation of the H-bonds and a distortion of the lactone ring, which is observed in bond lengths in the lactone ring. In the most favorable conformation for **2**, two H-bonds are formed between the hydroxyl groups and one between a hydroxyl group and carbonyl of the lactone ring. The DFT calculations result three respective conformations also for **3**: one with 4 H-bonds (3a), one with two H-bonds between C=O---HO (3b) and one with two H-bonds between RO---HO (3c). In this case, as well, the conformation, which has two H-bonds between the carbonyl and hydroxyl groups (3b) has the lowest energy.

Table SI4. Optimized DFT/b3lyp (6-311G(d,p)) structures for **1**, **2** and **3**: the number of H-bonds, total energies and energy differences for most favorable conformations.

Structure	Number of HBs	Direction of HBs	Energy (a.u.)	$\Delta E$ (kJ/mol)
<b>1</b>	4	counterclockwise	-2299.262198	-
<b>2a</b>	4	mixed	-2146.563559	14.16
<b>2b</b>	3	clockwise	-2146.568951	0
<b>2c</b>	3	counterclockwise	-2146.563908	13.24
<b>3a</b>	4	mixed	-1993.870797	24.86
<b>3b</b>	2	clockwise	-1993.880267	0
<b>3c</b>	2	counterclockwise	-1993.869361	28.63

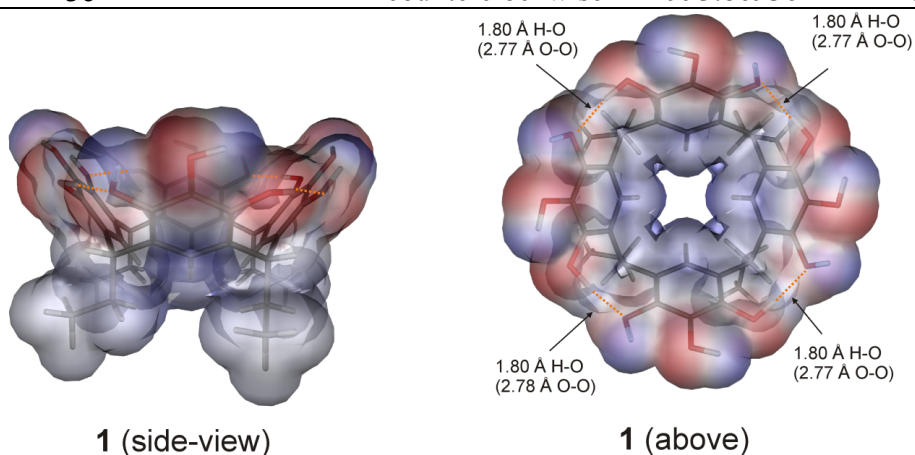
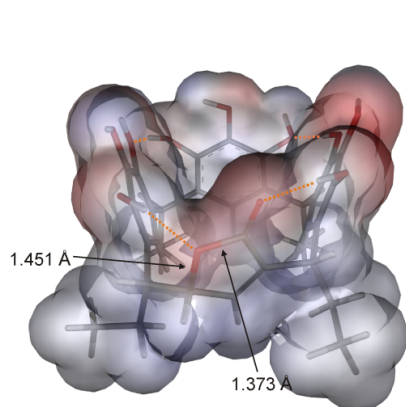
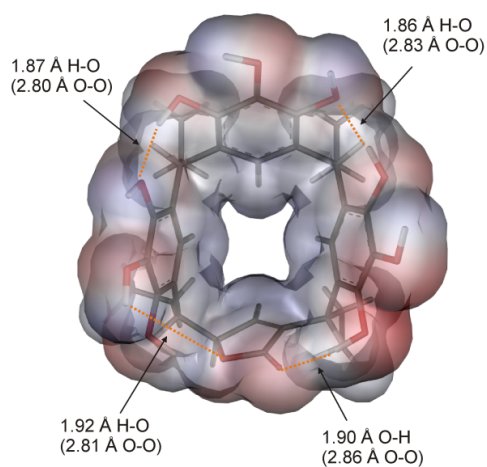


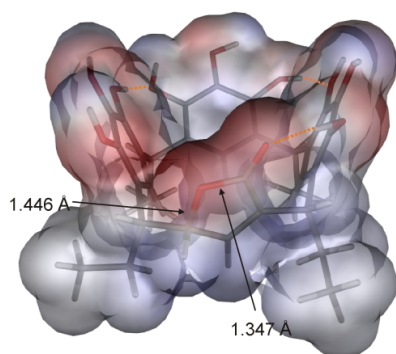
Figure SI12. DFT optimized structure for **1** (H-bonds marked with orange dotted line).



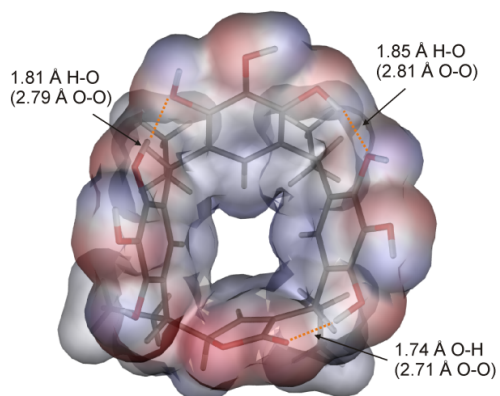
**2a** (side-view)



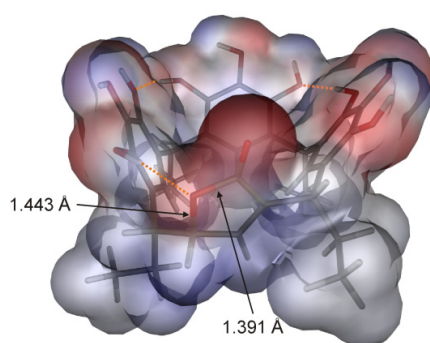
**2a** (above)



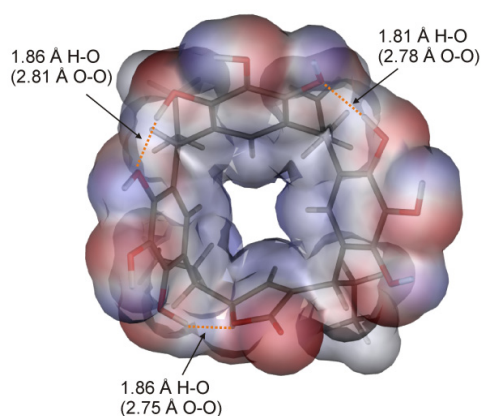
**2b** (side-view)



**2b** (above)



**2c** (side-view)



**2c** (above)

SI13. DFT optimized structures for **2** (H-bonds marked with orange dotted line).

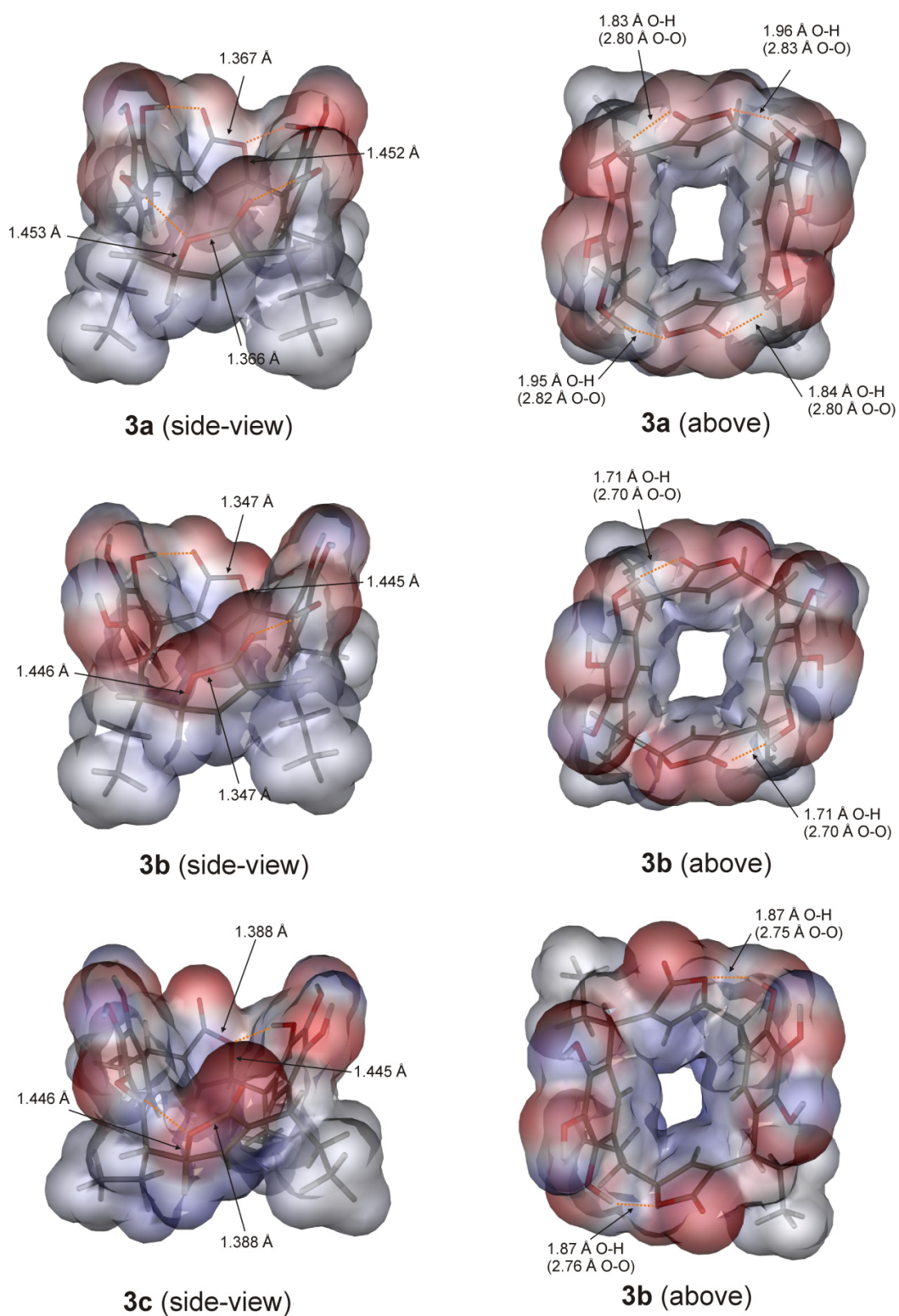


Figure SI14. DFT optimized structures for **3** (H-bonds marked with orange dotted line).

## 6. References

- [1] P. Timmerman, W. Verboom, D. Reinhoudt, *Tetrahedron* **1996**, *52*, 2663-2704.
- [2] L. J. de Koning, N. M. M. Nibbering, S. L. Van Orden, F. H. Laukien, *Int. J. Mass Spectrom. Ion Processes*, **1997**, *8*, 906-915.
- [3] Gaussian 09, Revision A.02, M. J. Frisch, G. W. Trucks, H. B. Schlegel, G. E. Scuseria, M. A. Robb, J. R. Cheeseman, G. Scalmani, V. Barone, B. Mennucci, G. A. Petersson, H. Nakatsuji, M. Caricato, X. Li, H. P. Hratchian, A. F. Izmaylov, J. Bloino, G. Zheng, J. L. Sonnenberg, M. Hada, M. Ehara, K. Toyota, R. Fukuda, J. Hasegawa, M. Ishida, T. Nakajima, Y. Honda, O. Kitao, H. Nakai, T. Vreven, J. A. Montgomery, Jr., J. E. Peralta, F. Ogliaro, M. Bearpark, J. J. Heyd, E. Brothers, K. N. Kudin, V. N. Staroverov, R. Kobayashi, J. Normand, K. Raghavachari, A. Rendell, J. C. Burant, S. S. Iyengar, J. Tomasi, M. Cossi, N. Rega, J. M. Millam, M. Klene, J. E. Knox, J. B. Cross, V. Bakken, C. Adamo, J. Jaramillo, R. Gomperts, R. E. Stratmann, O. Yazyev, A. J. Austin, R. Cammi, C. Pomelli, J. W. Ochterski, R. L. Martin, K. Morokuma, V. G. Zakrzewski, G. A. Voth, P. Salvador, J. J. Dannenberg, S. Dapprich, A. D. Daniels, O. Farkas, J. B. Foresman, J. V. Ortiz, J. Cioslowski, D. J. Fox, Gaussian, Inc., Wallingford CT, **2009**.